Medical Engineering and Physics 74 (2019) 89–98

Contents lists available at ScienceDirect

Medical Engineering and Physics

journal homepage: www.elsevier.com/locate/medengphy

Impedance and conductivity of bovine myocardium during freezing and thawing at slow rates - implications for cardiac cryo–ablation

G. Fischer[a,b,*], M. Handler[a,c], P.R. Johnston[c], D. Baumgarten[a,d]

[a] Institute of Electrical and Biomedical Engineering, UMIT - Private University for Health Sciences, Medical Informatics and Technology, Eduard-Wallnoefer-Zentrum 1, Hall in Tyrol 6060, Austria
[b] AFreeze GmbH, Innsbruck, Austria
[c] School of Environment and Science, Queensland Micro- and Nanotechnology Centre, Griffith University, Nathan, Queensland, Australia
[d] Institute of Electrical and Biomedical Engineering, Technische Universität Ilmenau, Ilmenau, Germany

ARTICLE INFO

Article history:
Received 9 January 2019
Revised 12 September 2019
Accepted 16 September 2019

Keywords:
Cryo-ablation
Tissue impedance
Osmotic virial equation
Electrode polarization

ABSTRACT

Increasing impedance during freezing might be a valuable marker for guiding cardiac cryo-ablation. We provide model based insights on how decreasing temperature below the freezing point of tissue relates to the percentage of frozen water. Furthermore, we provide experimental data for comparing this percentage with the increase in impedance.

Measurements were performed on a bovine tissue sample at frequencies between 5 and 80 kHz. Slow cooling and heating rates were applied to minimize temperature gradients in the myocardial sample and to allow accurate assessment of the freezing point. Computer simulation was applied to link impedance with temperature dependent conductivities. The osmotic virial equation was used to estimate the percentage of frozen water.

Measurements identified the freezing point at −0.6 °C. At −5 °C, impedance rose by more than a factor of ten compared to that at the freezing point and the percentage of frozen water was estimated as being 89%. At −49 °C impedance had increased by up to three orders of magnitude and ice formation was most pronounced in the extracellular space.

Progressive ice formation in tissue is reflected by a large increase in impedance, and impedance increases monotonically with the percentage of frozen water. Its analysis allows for experimental assessment of factors relevant to cell death. Solid ice contributes to the rupture of the micro-vasculature, while phase shifts reflect concentration differences between extra- and intracellular space driving osmotic water transfer across cell membranes.

1. Introduction

Within the past decade, cryo-ablation has gained significant importance as a treatment for supraventricular tachycardia and, in particular, for atrial fibrillation [1–4]. However, an inherent risk of cryo-ablation is unintended damage to healthy tissue by overfreezing [5]. With increasing use of cryo-thermal energy, reliable markers are needed for monitoring lesion formation and for protecting tissue structures adjacent to the thin-walled atrial myocardium [6]. In particular, phrenic nerve injury [7] and atrioesophageal fistulas [8] are documented complications related to unintended cooling or freezing of tissue adjacent to the left atrium.

Two decades ago, measurement of tissue impedance was proposed as a marker for monitoring the size of a frozen region of tissue during cryo-surgery [9]. An early in vitro study demonstrated that impedance could increase by more than three orders of magnitude in frozen tissue [10]. However, only recently have devices been developed that allow in vivo assessment of impedance during cardiac cryo-ablation. In [11], two ring electrodes on a cryo-balloon catheter were used for assessing the increase of electrical impedance during ice formation in pulmonary vein ablation. It was shown that impedance increases with progressive ice formation and may be a reliable marker for the actual dimension of frozen tissue. It was also found that the increase of impedance was related to the outcome of the procedure. Clinically important conditions such as the actual placement of a cryo-balloon within the pulmonary vein had significant impact on impedance. For effective freezes, impedance rose by up to almost 10 kΩ, whereas for ineffective freezes, the increase was only of the order of some tens or a few hundred ohms.

* Corresponding author. at: Institute of Electrical and Biomedical Engineering, UMIT - Private University for Health Sciences, Medical Informatics and Technology, Eduard-Wallnoefer-Zentrum 1, Hall in Tyrol 6060, Austria
E-mail address: gerald.fischer@umit.at (G. Fischer).

https://doi.org/10.1016/j.medengphy.2019.09.017
1350-4533/

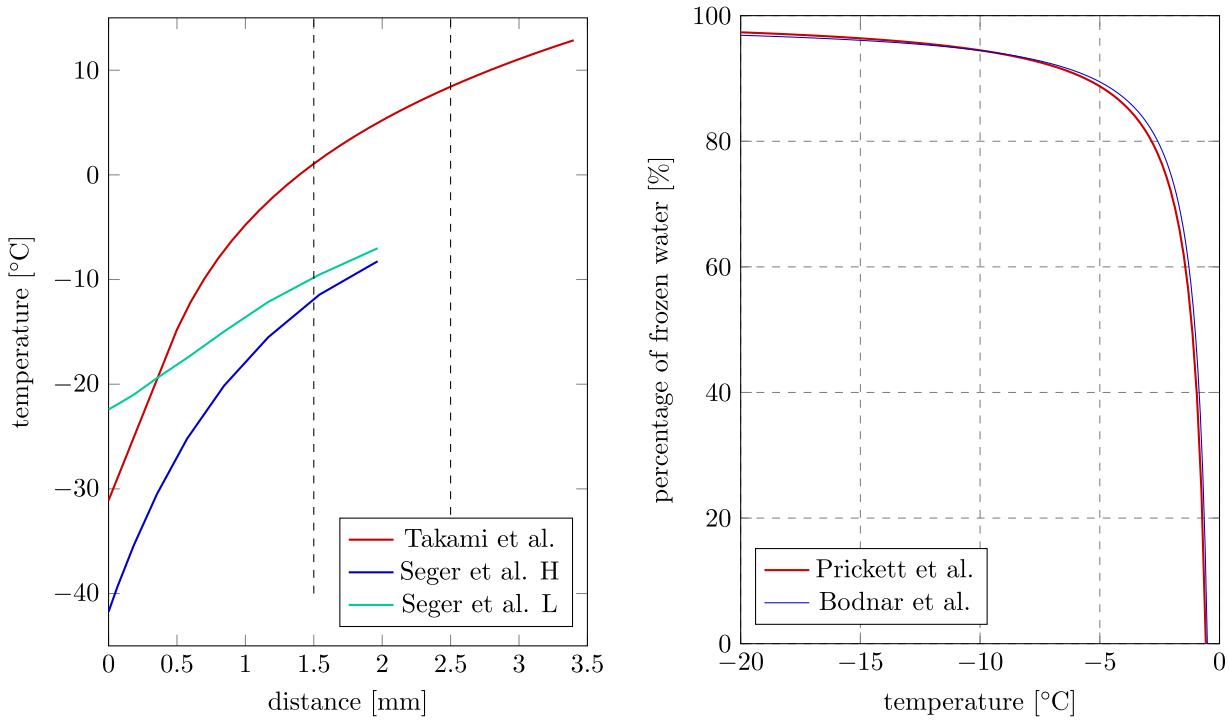

Fig. 1. *A:* Stationary temperature profiles across the atrial wall. The red line depicts the experimental data from [16]. The blue lines depict simulated traces from [14], in segments of high (H) and low (L) cooling power, along a circumference of a loop catheter. Dashed vertical lines mark the typical thickness of the atrial wall ranging from 1.5 mm to 2.5 mm. *B:* Percentage of frozen water in an electrolyte at thermodynamic equilibrium. The blue line is the result obtained for the osmotic virial equation [19] (see Appendix A). The red line is the result obtained for physiological saline solution [36]. (For interpretation of the references to colour in this figure legend, the reader is referred to the web version of this article.)

To develop methods that accurately relate the increase of impedance to a thickness or other dimension of the ice layer, a clear understanding of how freezing affects electrical conduction in tissue is needed. An early study investigating the variation of impedance with rapid cooling down to temperatures between −100 °C and −60 °C reports a quick increase ("jump") of impedance by up to four orders of magnitude [10]. This contributed to the over-simplified picture that frozen tissue is essentially non conducting [12]. However, for atrial cryo-ablation such extremely low temperatures might even potentially be harmful, as they involve the risk of unintentionally destroying adjacent tissue.

Thus, in order to promote the use of impedance monitoring in cardiac cryo-ablation, it is necessary to provide a better understanding of, and accurate data for, impedance and conductivity of the myocardium in the temperature range of interest. In our study, we provide an experimental setting that allows for measurement of myocardial impedance from body temperature down to −50 °C. In particular, we focus on an accurate assessment of the freezing point (i.e. the onset of ice formation) and the bio-physical mechanisms driving the increase of impedance at temperatures down to approximately −20 °C. We also provide conductivity data that can be used for computer models of cardiac cryo-ablation [13,14]. Furthermore, we investigate the effect of promoting ice formation on electrode polarization at the tissue contact surface [15]. Appendices, which contain detailed information on the methodological background, are provided as an online supplement.

2. Biophysical background

2.1. Temperature profile

In order to plan the experimental setting, a literature review on the biophysical background of cryo-ablation within the human atrium was performed. Fig. 1A shows examples of temperature profiles across the atrial wall near steady state freezing (i.e. after at least 90 s of freezing). One trace is a fit of a logarithmic temperature function to experimentally measured temperature profiles obtained from more than 50 cryo-balloon ablations in dogs. Takami et al. [16] fitted the logarithmic function to 259 observation points at distances of 0.5 to 25 mm from the balloon. At the point of contact between the balloon surface and the endocardium, the mean steady state temperature was near -31 °C. In Fig. 1A, a linear interpolation was performed from the surface to the logarithmic function of Takami et al. Note that the logarithmic function is a mean representation of successful and non-successful freezes. It can be concluded from Takami et al. that in successful freezes the temperature may be up to 20 °C below the logarithmic function.

Also in Fig. 1A, two temperature functions for a loop-shaped cryo-ablation catheter are shown that are obtained from computer simulations performed by our group. The simulations conducted by Seger et al. [14] were compared with cryo-lesions created by cryo-ablation in the pig atrium. Due to varying refrigerant distribution along the circumference of the loop, temperature profiles for maximal and minimal refrigerant distribution are shown. The lowest temperature at the contact of the loop surface with the endocardium was near −40 °C, rising to about −10 °C at the epicardium.

The typical wall thickness of the human left atrium is in the range of 1.5 mm to 2.5 mm [17]. As can be seen from all traces in Fig. 1A, a huge mean temperature gradient of more than 10° mm^{-1} is observed across the relatively thin atrial wall. Such huge temperature gradients can also be observed in other applications of cryo-ablation [13,18].

2.2. Freezing point

Extra- and intracellular body fluids are aqueous multicomponent electrolytes. As was shown by Prickett and co-workers [19], the freezing point of such electrolytes displays little dependency on the actual composition of solvents but depends mainly on their

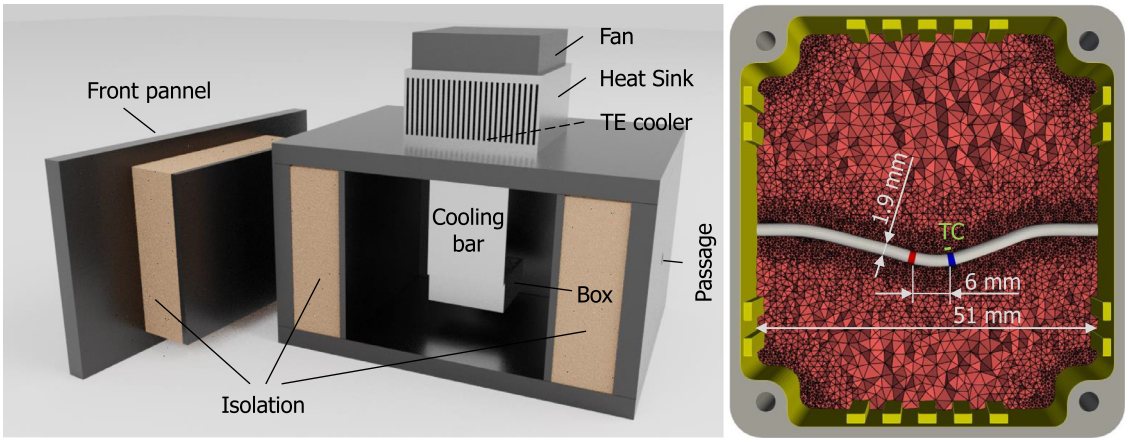

Fig. 2. Schematic experimental set-up. *Left:* A metallic box with the tissue sample was placed inside an isolated housing. An aluminum bar was used for thermally connecting it with a thermoelectric (TE) cooler (not visible) on the top of the housing. An isolated passage was built for introducing the catheter and thermocouple (TC). *Right:* Dimensions of the metallic box together with the catheter.
Note that the catheter was slightly curved due to the preparation in the box. For finite element simulations the volume filled by tissue was discretised by tetrahedral elements. Mesh grid is shown at the catheter level for illustration.

osmolality. At isotonic osmolality (308 mmmol kg^{-1}), a freezing point of −0.6 °C is obtained. Pure water freezes entirely at its freezing point, but electrolytic solvents do not freeze entirely at their freezing point. When lowering temperature somewhat below the freezing point, some percentage of the water freezes within the electrolyte. This increases the osmolality of the remaining liquid electrolyte such that it is in thermodynamic equilibrium with the actual temperature. Thus, with decreasing temperature, the percentage of frozen water in the body liquids increases.

The osmotic virial equation proposed by Prickett et al. [19] allows for a reasonable estimation of the thermodynamic equilibrium temperature. As shown in Appendix A, the percentage of frozen water in the tissue (see Fig. 1B) can be calculated. At −1.2 °C, half of the water is frozen at the thermodynamic equilibrium and at −5.0 °C, 89% of the water is frozen.

As the freezing of water drives an increase of impedance during progressive cooling, Fig. 1B suggests that slightly below the freezing point, significant changes of impedance are observed within a range of a few degrees centigrade. Thus, the high spatial thermal gradients (>10 °mm^{-1}) that are observed during in vivo cryo-ablation (Fig. 1A) will also induce large spatial resistivity gradients in the tissue. This creates enormous difficulty for the accurate measurement of local tissue temperature and local resistivity in vivo. Therefore, we decided to use in vitro experiments for assessing the temperature dependence of impedance. We aimed to keep temperature gradients small within the probe. As shown in Appendix B, low cooling or heating rates are needed for achieving a uniform temperature distribution.

3. Methods

3.1. Thermal protocol

An Image of the experimental setup is shown in Fig. 2. Bovine myocardial tissue (51 g) was placed in a metallic box with a volume of 70 cm^3. To avoid non-conducting air inclusions between patches of tissue, 10 g of physiological saline solution was added. A standard 6 Fr (french size) diagnostic electrophysiology catheter with Platine electrodes of 1.9 mm diameter and 1.0 mm width was placed in the middle of the box as shown. Two electrodes at the center of the box were spaced at a distance of 6.1 mm and used for measuring impedance.

The box containing the tissue was made from aluminum of 1.5 mm thickness to reduce temperature gradients. A bar of 60 mm × 3 mm aluminum was used for thermally connecting the box with a thermoelectric (TE) cooling device (FTA 951, Ferrotec Corporation). The cooling power of the TE cooler was continuously varied by adjusting the current between 0 and 6A. To reheat the tissue to body temperature, the polarity of the current was reversed and to provide thermal isolation, the tissue box and TE cooler were mounted inside an insulated box. TE-cooling alone allowed for cooling down to approximately −20 °C. In order to achieve lower temperatures, the air outside the insulated box was enclosed in a plastic housing and pre-cooled down to approximately −15 °C using dry ice (solid CO_2). Thus, temperatures down to −50 °C were achieved in the tissue. A thermocouple of Type K, with a length of 2 mm, was placed parallel to the catheter axis approximately 1 mm from one of the two recording electrodes. A calibrated logger (GMH 3210-GH, Greisinger GmbH) was used to continuously measure the temperature. According to the calibration protocol the accuracy of the temperature readings was ±0.1 °C.

Bovine myocardial tissue was obtained from a certified animal lab in frozen condition. Before starting the experiment, the tissue was allowed to thaw for 1 h. During the thawing time, the tissue was cut from the ventricle and placed in the metallic box. To avoid any degeneration of the tissue at warm temperatures, rewarming was allowed up to 10 to 15 °C, which also ensured that no regions of frozen tissue existed at the beginning of the experiment. Then the temperature was decreased slowly (average gradient −6 °C/hour) to ensure that temperature gradients inside the tissue were small (see Appendix B). When crossing the freezing point (−0.6 °C), cooling power was kept constant for 30 minutes to guarantee a slow and homogeneous formation of ice inside the tissue. Then cooling was continued down to approximately −50 °C.

The tissue was maintained at the lowest temperature for 30 min and then slowly rewarmed (average gradient +0.6 °C/h) up to 10 °C. To avoid degeneration of the thawed tissue, further warming up to body temperature was performed quickly (15 minutes), with a waiting period of 5 minutes for equilibration of the tissue temperature to near body temperature. The entire experiment took about 24 h.

3.2. Impedance measurements

To allow impedance to be measured at conditions comparable to an electrophysiology laboratory, a standard EP cable (length 150 cm) was used to connect a standard 6 Fr decapolar diagnostic catheter (length 115 cm) to the impedance registration circuit. The output voltage of a function generator (TG315, TTi) was set to 10Vpp (±1%). During the cool down phase, measurements were

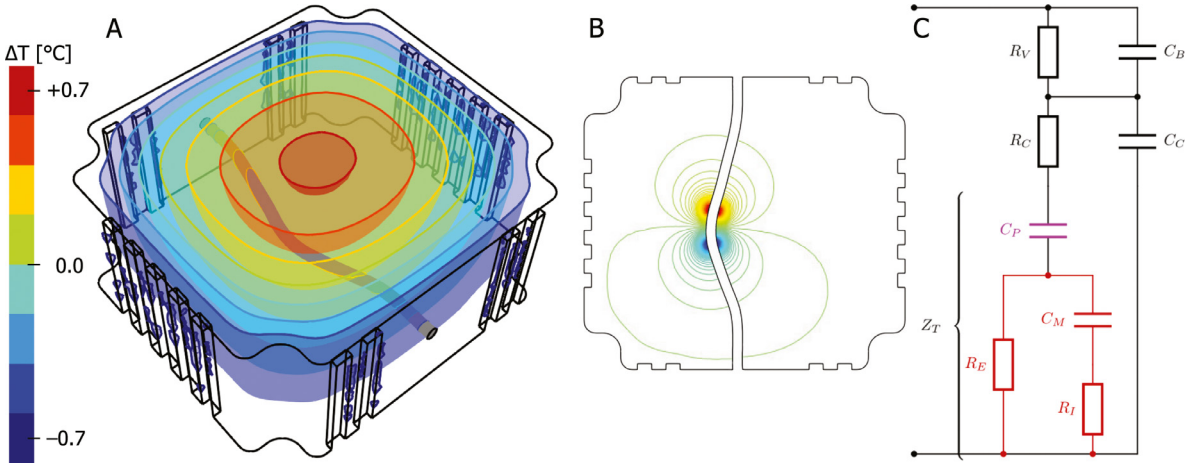

Fig. 3. *Panel A:* Simulated spatial temperature profile at a constant cooling rate of −6 °C/h. As cooling is applied via the metallic housing, the outer tissue layers are warmer compared to the center.
Note that at a constant cooling rate absolute temperature is time dependent. Thus, we display the relative temperature difference ΔT, which is stationary for a constant cooling rate. Isosurfaces are shown in steps of 0.2 °C. The difference between the cooler outer border and the warmer tissue center is 1 °C (see also Appendix B). *Panel B:* Finite element model of the potential field inside the metallic box. A constant current was applied across the two electrodes and the potential field was computed. Assuming unit conductivity (1S m^{-1}) an impedance of 171 Ω was obtained. This value was used for converting the measured impedance into its corresponding conductivity (see Appendix D). *Panel C:* Equivalent circuit diagram of the experimental set-up. On the registration board the resistor R_V was used for creating a voltage divider structure. The parasitic board capacity C_B is in parallel to R_V. The resistance of the cable R_C is in series with the tissue impedance Z_T. Tissue impedance Z_T is modeled by four *RC* components as described in the text. The parasitic cable capacitance C_C is in parallel to Z_T and R_C.

performed at 5 kHz, 20 kHz and 80kHz (all frequencies ±1%) and during rewarming, data were recorded at 20 kHz for control purposes. The resulting data were then digitized using a digital oscilloscope (IDS-6052-U, Isotech). A circuit equivalent to the experimental setting is shown in Fig. 3C. Parasitic properties (capacitance/resistance) of cables and boards were assessed using the same equipment.

3.3. Computation of parameters

The tissue impedance Z_T was calculated at each temperature and frequency from the measured data using standard AC-circuit calculations. The equivalent circuit model depicted in Fig. 3C was used to further describe the electrical properties of the tissue. Similarly, as described elsewhere ([20,21]), the resistors $R_E(T)$ (extracellular conduction), $R_I(T)$ (intracellular conduction) and the capacitance $C_M(T)$ (cell membrane) were used to model conduction in the beta-dispersion band. As body liquids exhibit a strong ionic conductivity, electrode surface polarization was modeled by a capacitance $C_P(T)$ similar to that describe elsewhere ([15]).

The following approach was used to compute the parameters $R_E(T)$, $R_I(T)$, $C_M(T)$ and $C_P(T)$ as a function of temperature. At each of the 3 frequencies (5kHz, 20kHz and 80kHz) a spline fit (cubic Hermite splines) was created to obtain a continuous approximation of the temperature dependent tissue impedance $Z_T(T, f)$. Then, a linear optimization scheme (Broyden–Fletcher–Goldfarb–Shanno Algorithm) was implemented to compute the temperature dependent parameters in steps of 0.05 °C.

A finite element model of the experimental setting was created (see Fig. 3A and B) to link the measured and computed impedances to tissue conductivity. The impedance Z_1 obtained for a hypothetical conductivity of 1 S m^{-1} was computed. This impedance defines a conversion factor that can be used for converting the measured temperature dependent impedance into a temperature dependent tissue conductivity or resistivity (see Appendix D).

4. Results

4.1. Thermal protocol

In Fig. 4 tissue temperature is depicted as a function of time. As can be seen from the insert, moderate subzero temperatures were obtained approximately 2.5 h after starting the experiment. After reaching -0.8 °C, the temperature rose back to -0.6 °C while cooling power (i.e. 2A current across the TE-cooler) was kept constant. From the local minimum, it took 90 min to decrease the temperature to −0.9 °C, indicating that crystallization nuclei formed at −0.8 °C trigger ice formation. Then, initial growth of ice occurred at −0.6 °C. As can be seen from Fig. 1B, a significant percentage of water freezes initially within a narrow temperature range. Thus, a distinct holding point of temperature was observable when initial freezing occurred.

The lowest temperature obtained was −49.1 °C. During rewarming a holding point was observed again near the freezing point at moderate subzero temperatures.

Table 1
Parameters for the equivalent circuit.

Parameter	Value	Temperature range
R_V	330 Ω	$-1.5\ °C < T$
R_V	10 kΩ	$-15\ °C \leq T \leq -1.5\ °C$
R_V	100 kΩ	$-15\ °C < T$
R_C	5 Ω	all
C_B	2.3 pF	all
C_C	228 pF	all

4.2. Impedance measurements

Parameters for the serial resistors used in the measurement procedure are listed in Table 1 together with the parasitic properties of the board (C_B) and cables (C_C) that were determined. Note that the values of the serial resistors were increased with progressive freezing of the tissue in order to account for the increasing tissue impedance at low temperature. The temperature dependent tissue impedance obtained from the experiment is plotted in Fig. 5 on a semi-logarithmic scale. When cooling from body temperature down to the freezing point, an increase of impedance was observed. In the semi-logarithmic plot, the temperature dependence of impedance appears approximately linear. This is consistent with the known temperature dependence of electrolytic conduction. Cooling the tissue from body temperature down to −0.6 °C increased the impedance by a factor of approximately 2.5.

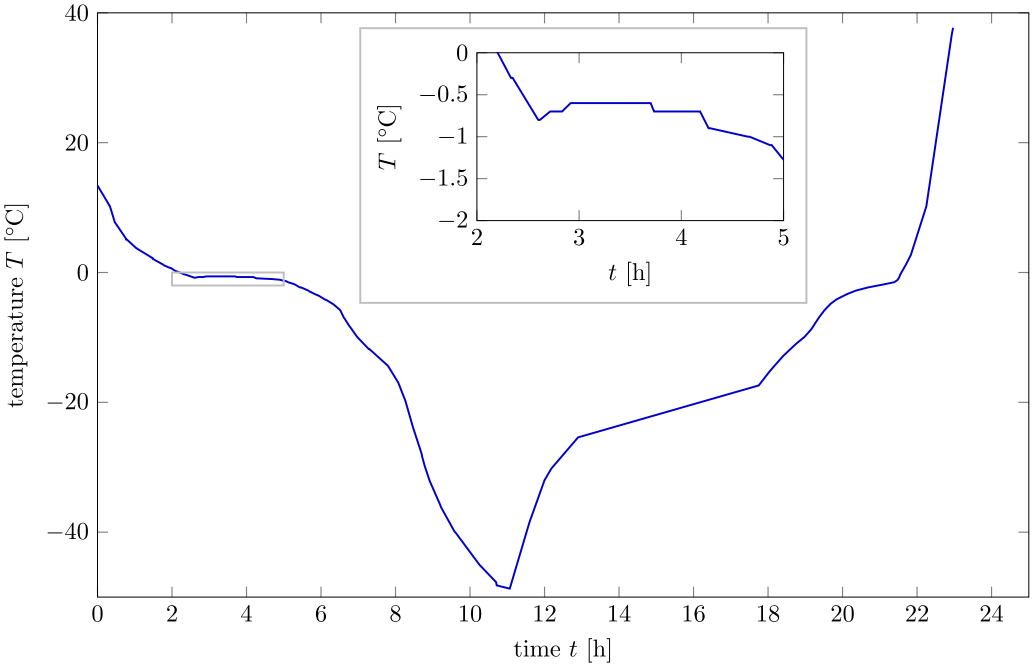

Fig. 4. Tissue temperature as a function of time during cooling and rewarming.
Note that time base is labeled in hours. The insert zooms the local temperature minimum followed by a holding point which was observed when crossing the freezing point at −0.6 °C.

As can be seen from the insert in Fig. 5, during initial ice formation (temperature range −0.6 °C to −0.9 °C, see also insert in Fig. 4) no significant increase of impedance was observed. When the temperature dropped below −0.9 °C a significant increase of impedance occurred. Impedance rose by one order of magnitude with progressive freezing within a narrow temperature range (−0.9 °C to −4.5 °C). This suggests that a high percentage of water froze within this temperature range and only a small percentage of water was still liquid at around −5 °C. With further cooling, the slope flattened. At 5kHz and 20 kHz an increase by another order of magnitude was obtained within the interval of −4.5 °C to −15 °C. At 5kHz an increase by a third order of magnitude was observed for temperatures down to −50 °C.

At low temperature, the parasitic capacitance of the EP-cable and the catheter itself had a significant impact on the recorded data. At 20 kHz and −15 °C, the impedance of the parasitic

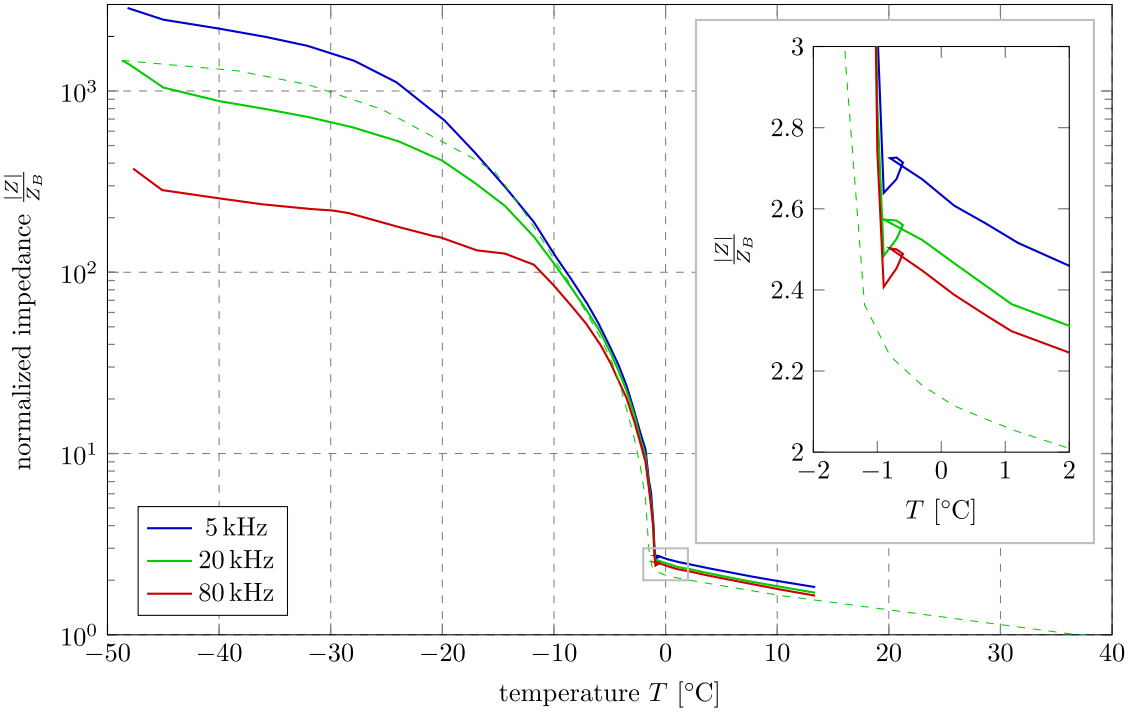

Fig. 5. The magnitude of measured tissue impedance, normalized by the value obtained at body temperature, plotted as a function of temperature. The three solid lines display the results obtained during cooling for the three test frequencies. The dashed green line is the impedance during rewarming at 20 kHz. The insert zooms impedance in a temperature range near the freezing point (−0.6 °C).

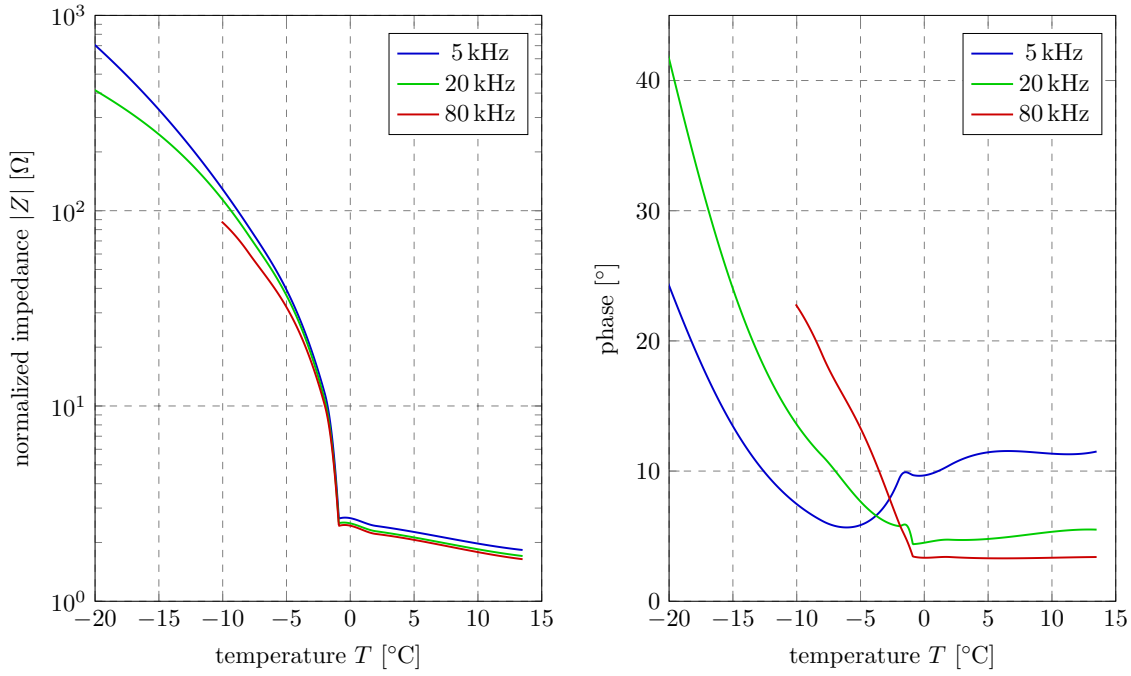

Fig. 6. *Left:* The magnitude of fitted normalized tissue impedance during cooling for the three test frequencies. *Right:* Phase of the fitted tissue impedance during cooling for the three test frequencies.
Note that above the freezing point, the lowest frequency displays the largest phase shift. When crossing the freezing point, the lowest frequency displays the lowest phase shift. For all frequencies, the phase shift increases with progressive freezing.

Table 2
Normalized impedance $\frac{Z}{Z_B}$ at the three test frequencies.

	5 kHz		20 kHz		80 kHz	
Temperature	$\frac{\lvert Z\rvert}{Z_B}$	arg Z	$\frac{\lvert Z\rvert}{Z_B}$	arg Z	$\frac{\lvert Z\rvert}{Z_B}$	arg Z
10 °C	1.97	11.3°	1.85	5.3°	1.79	3.3°
5 °C	2.26	11.4°	2.12	4.8°	2.06	3.3°
0 °C	2.66	9.7°	2.50	4.5°	2.44	3.3°
−5 °C	39.4	5.9°	36.8	7.7°	32.0	13.3°
−10 °C	129	7.5°	114	13.6°	87.0	22.7°
−15 °C	329	13.5°	246	24.0°	–	–
−20 °C	704	24.2°	414	41.7°	–	–

capacitance in parallel with the tissue had approximately the same impedance as that of the tissue itself. Thus, with progressive cooling to temperatures well below −15 °C, the increase in tissue impedance was partially masked by the parasitic parallel capacitance.

4.3. Computation of parameters

Fig. 6 shows the computed spline fits for the impedance data. In order to account for the fast increase of impedance below the freezing point, the splines were allowed to kink (have a discontinuous first derivative) at −0.9 °C. At the highest test frequency (80 kHz) the parasitic cable capacitance C_C, had a reactance of approximately 90 kΩ. Below −10 °C, the computed tissue impedance at 80 kHz was more than four times larger than the cable reactance. Here, the experimental estimates were of low accuracy and these results are not shown in the plot. Note that the phase shift increased with progressing ice formation. For selected temperatures, the impedance is listed in Table 2.

The data obtained from spline interpolation was used for computing the *RC* components of the equivalent circuit, as defined in Fig. 3C, and the results are shown in Fig. 7. Above the freezing point, the extracellular resistance R_E was smaller than the intracellular resistance R_I (in series with membrane capacitance C_M). Hence, the majority of the current flow was across the extracellular space, which is in series with the polarization capacitance C_P. This explains why in Fig. 6B the lowest frequency displayed the largest phase shift above the freezing point.

Below the freezing point, extracellular resistance R_E increases more rapidly with decreasing temperature than does intracellular resistance R_I. Hence, the contribution of the intracellular pathway to the total current flow increased. Here, the contribution of the $R_I C_M$ pathway also increased with increasing frequency. This explains why in Fig. 6B the highest frequency displayed the largest phase shift well below the freezing point.

We applied the finite element model shown in Fig. 2 to convert the four estimated *RC* parameters of the equivalent circuit to the conductivity values (see Appendix D). This provides suitable data for computer simulations. The validity of this conversion is checked by comparing results obtained at body temperature with values listed in the literature.

Extracellular ohmic conductivity was estimated to be 0.65S m^{-1}. This value was larger than the expected value (mean 0.18S m^{-1} in [22]) as a 16% physiological saline solution was added to avoid air inclusions. At body temperature, the conductivity of physiological saline solution is 1.8S m^{-1} (see [23] and Appendix E) and, thus, about ten-fold the value of the extracellular myocardial space. This explains why our estimation is above the expected value. As can be seen from Appendix E, the relative increase of impedance with progressive freezing of a saline solution qualitatively matches the results obtained for the tissue, and the saline solution behaves like an ohmic conductor in the liquid and (partially) frozen state.

Intracellular ohmic conductivity was estimated to be 0.1S m^{-1}. This value is near the expected value (mean 0.09S m^{-1} in [22]).

As shown in Appendix C, the estimated polarization capacitance is in a plausible order of magnitude. Note that polarization is a property of the electrode-tissue interface. Relative to a surface unit, a value for the polarization capacitance of 200 nF mm^{-2} was obtained. The computed membrane capacitance was converted to a relative tissue permittivity, ϵ_r, as described in Appendix D, giving an estimated value of $\epsilon_r = 2 \times 10^4$. In the report by Skourou

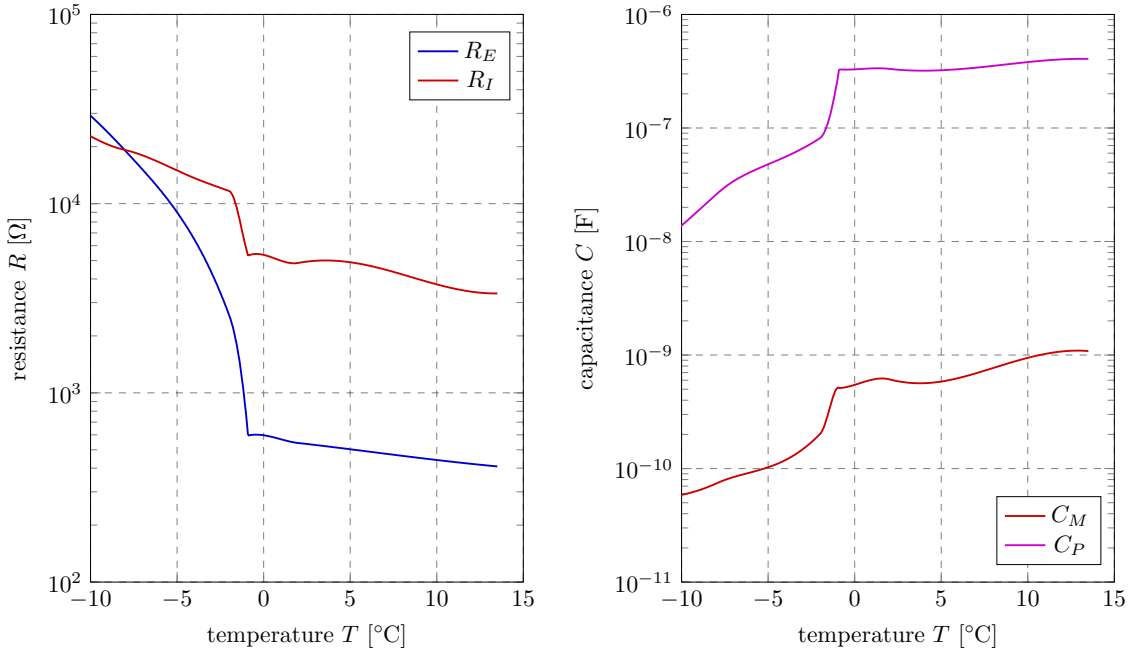

Fig. 7. *Left:* Extra- and intracellular resitance (R_E and R_I) as a function of temperature during cool down.
Note that extracellular resistance grows much faster with progressive freezing than intracellular resistance. *Right:* Polarization capacitance C_P and membrane capacitance C_M as a function of temperature during cool down. Both capacitances decrease during freezing.

et al. [24], tissue permittivity of rat skeletal muscle is investigated, where it is shown that the relative permittivity displays a strong dependence on frequency values in a range of 1×10^5 Hz. Hence, our estimation is within a plausible range.

5. Discussion

5.1. Tissue temperature and progressive ice formation

In this work, we investigated the change of impedance and conductivity in bovine myocardium during freezing. To reduce the influence of temperature gradients inside the tissue, we performed measurements at slow cooling and slow heating rates. This allowed the electrical conduction of partially frozen body liquids to be accurately assessed. Our results suggest that the following temperature ranges may be distinguished.

From body temperature down to the freezing point a continuous increase of impedance by a factor of 2.5 was observed. This increase was caused by the well known temperature dependent conduction properties of a liquid electrolyte [23].

At −0.8 °C ice formation started and the release of enthalpy by the formation of ice-particles caused a moderate rewarming to −0.6 °C. The experimental observation of such a local temperature minimum below the freezing point is a well-known phenomenon [13]. The moderate elevation of 0.2 °C obtained in our experiment indicates a very slow formation of ice. The local temperature maximum at the freezing point corresponds to the prediction of the osmotic virial equation [19] for a multisolute electrolytic solution at isotonic osmolality (−0.6 °C at 320 mmol/kg) within the resolution of the temperature sensor.

Surprisingly, during initial freezing (i.e. the temperature plateau in the 90 minutes between the onset of freezing and −0.9 °C) impedance remained almost constant. A small but measurable decrease in impedance of 3% was observed. As can be estimated from the osmotic virial equation [19], cooling to 0.3 °C below the freezing point of an isotonic solution freezes approximately 25% of the water. This suggests that a relatively small percentage of frozen water (significantly less than 50%) may not be sufficient for observing a noticeable increase of impedance. As the volume portion containing liquid electrolyte decreases, the ion concentration increases. At low (near isotonic) concentrations, conductivity is approximately proportional to concentration. These two effects may largely cancel each other out, which explains the almost constant value in this range.

As can be seen from Appendix E, the small drop of impedance observed during initial freezing may be caused by a diffusion of ions. The slow cooling rates we applied in our experiments allowed for the observation of a slow diffusion process. It is questionable whether this effect may be observable or relevant for clinical cryo-ablation where much faster cooling rates are applied. With respect to cryo-ablation therapy, it is an important finding that, below −1.0 °C, impedance rises quickly by more than one order of magnitude within a relatively narrow temperature range of 4 °C. Once a sufficiently large percentage of water is frozen, only narrow and long conducting channels remain for conduction. Furthermore, when ion concentration in the liquid electrolyte reaches a saturation level, conductivity of the electrolyte does not increase further.

At −5 °C, impedance is increased by more than an order of magnitude compared to the impedance observed at the freezing point. There is a monotonically increasing relation between the percentage of frozen water and impedance. From the osmotic virial equation it can be estimated that 89% of water in the body liquids are frozen at −5 °C.

Within a temperature interval from −5 °C down to −15 °C, a further increase of impedance by another order of magnitude occurs when recording at 5kHz, reflecting further ice formation. Below −15 °C, the increase of impedance with progressive cooling further flattens but a continuous increase was observed down to −50 °C. At 5kHz and −50 °C, the increase of impedance is almost three orders of magnitude higher than the impedance at the freezing point. As will be discussed in more detail below, our experimental setting did not allow for an accurate assessment of impedance at very low temperature as the parasitic capacitance of the catheter and EP cable largely masks very high tissue impedance.

When comparing the data recorded at 20 kHz for freezing and thawing, a slight hysteresis was observed in the data at temperatures below -15 °C. Most likely this hysteresis was due to residual temperature gradients in the tissue. During cooling, the tissue was somewhat warmer at the center of the tissue mass compared to the boarder. During rewarming, this gradient reversed and this may account for the differences observed. As can be seen from Fig. 4, relatively high cooling and rewarming rates were obtained in the temperature range below −15 °C due to the use of dry ice. After complete melting, impedance returned close to the value obtained at the beginning of the experiment, but impedance was consistently lower by about 10%. Most likely this was caused by irreversible changes inside the tissue during the experiment. Mechanical forces due to freezing and thawing may have ruptured cell membranes and lowered impedance by direct access of ohmic current flow to the intracellular space, an effect that was noted also by Yu et al. [25]. Furthermore, diffusion of ions may have occured during the experiment which can also alter the conductivity.

By measuring impedance at three test frequencies, it was possible to investigate temperature dependent extra- and intracellular conductivity. Extracellular resistance rose much more quickly than the intracellular resistance. It is a well described phenomenon that water in the intracellular space freezes at lower temperature [25–27], and the observed difference of relative increase of extra- and intracellular resistance may reflect osmotic gradients across the cell membrane.

5.2. Relevance for myocardial ablation

No definitive conclusion can be found from the literature about the temperature that is required for the controlled triggering of cell death (necrosis or apoptosis) in cardiac tissue during cryo-ablation. As a coarse indicator, a temperature of −20 °C, maintained for at least one minute, is considered to be lethal for muscle tissue [26,28]. However, the data presented by Takami et al. [16] suggest that even significantly warmer temperatures may be sufficient for creating a cryo-lesion in atrial tissue. Fig. 1 depicts a temperature-distance curve taken from the report by Takami et al. [16]. These data contain successful and incomplete ablations. As reported by Takami and colleagues [16], temperature was preferentially some degrees of centigrade below the trace, and the ablation time was at least 90 s for successful ablation. This suggests that moderate subzero temperatures might be sufficient for epicardial lesion formation. Furthermore, a computer model of a cryo-loop catheter described by Seger et al. [14] predicts moderate sub-zero temperatures at the epicardium. Also, for such cryo-loop catheters, successful pulmonary vein isolation has been demonstrated in humans [4,29]. Recently, transmural ice formation was confirmed clinically for a loop catheter [6].

Our data and the work by Prickett et al. [27] suggest that at around −5 °C a significant portion of water (near 90%) is frozen in the tissue. Such a significant portion of frozen water might contribute to cell death. Ice formation in the micro vasculature induces rupture of tiny vessels by shear forces due to freezing and thawing of ice [28]. Furthermore, ice formation in the extracellular space creates osmotic gradients at the cell membrane [27]. Both effects promote cell death. Obviously, our data recorded in an in vitro setting do not allow us to finally define a lethal temperature for cardiac tissue. However, our results indicate that at −5 °C ice formation may be sufficient for potentially promoting myocardial cell death by rupture of micro vasculature and osmotic effects.

As can be seen from Fig. 1, huge temperature gradients occur inside the atrial wall during cryo-ablation. The mean temperature gradient across the atrial wall is typically in the order of $10^{\circ}\ mm^{-1}$. This poses an enormous challenge for accurately measuring local tissue temperature in vivo. In experimental settings, temperature sensors are often attached to a catheter or probe. The rapid increase of temperature within a few millimeters from the probe might be underestimated. This may explain why lethal thresholds might be significantly warmer than the −20 °C reported elsewhere ([26,28]).

5.3. Cooling rate

We performed the experiment at an extremely low cooling rate ($6^{\circ}C\ h^{-1}$). The reason for choosing such a low rate was to avoid large temperature gradients in the tissue. As is shown in Appendix B, the ratio of the high heat capacity of tissue (significant water content) and its low thermal conductivity generates relative large gradients during cooling. Only at sufficiently low cooling rates do they become small enough to establish an accurate temperature to impedance relationship. As can be seen from our treatment, the size of the tissue patch also has significant impact on the temperature difference ΔT. Our concept of using a standard diagnostic catheter for assessing impedance required a large tissue sample. In future studies, micro-electrodes may be used in combination with small tissue volumes for accurately assessing the temperature to impedance relation at much faster cooling rates.

The computation of a temperature dependent percentage of frozen water in tissue (given in Appendix A) assumes that the saline solution is in thermal equilibrium. As reported by Han and Bischof [30], the geometric dimension of ice crystals formed in a saline solution is in the order of 100μm. Furthermore, the small dimensions of cell structures in tissue may also contribute to reducing the size of crystals. At such small dimensions, thermal equilibrium can be achieved at relatively short time constants. In early in vitro studies [10,25], cooling rates were approximately 200 times faster than in our study. Quick responses of impedance with time constants in the order of 10s were observed. However, at such fast rates no accurate temperature to impedance relationship was obtained. Similarly, an in vivo study showed that within 90s clinically relevant changes of impedance (prediction of a successful ablation) can be observed [11]. These experimental findings indicate that thermal equilibrium inside frozen tissue may occur at much shorter time constants such as those that were applied in our experimental setting. Thus, the accurate temperate to impedance relationship we established may be used for simulating cardiac cryo-ablation at clinically relevant time scales. Here, future experimental validation is needed.

5.4. Catheter temperature vs. impedance

Cryo-catheters available for routine cardiac ablation use temperature sensors which are located inside the catheter. Thus, depending on the type of catheters, temperatures down to −80 °C and even below are measured [4,13], while tissue temperature is significantly warmer. For example, when using a catheter with a metallic tip for ablation near the AV-node, a temperature of −30 °C inside the tip is recommended for avoiding irreversible ablation of the AV-node (cryo-mapping [31]). However, −30 °C inside the tip may correspond to a significantly warmer, positive temperature at the AV-node when considering temperature gradients from tip to tissue. Cryo-balloon catheters measure the temperature of the boiled refrigerant near the center of the balloon, more than 1cm away from the target tissue.

Thus, while users are asking for reliable parameters that allow for monitoring of ice formation, temperature readings are poorly linked to the true tissue temperature. Electrodes that allow for safe recording of electrograms are in widespread clinical use and can also be used for cryo-impedance recordings. In contrast to temperature, which is local information at an observation site, impedance is an integral of temperature dependent conductivity across the

atrial wall. In other words, a temperature field within the tissue is linked with a conductivity field in the tissue. Impedance recorded by a cryo-ablation catheter, thus, represents a weighted mean of ice formation within the tissue. This will allow for much more accurate monitoring of ice formation during freezing. Furthermore, during thawing, after termination of a freeze, impedance should also allow for reliable detection of melting. Note that a catheter should not be moved before it is entirely disconnected from the tissue.

Impedance will depend on the shape and size of an electrode. Future work is needed to gain insight as to how impedance varies during in vivo ice formation, when spatial and temporal gradients occur. Our data analysis provides a temperature dependent model of tissue conductivity, which also contains an approximation to the temperature dependent electrode polarization capacitance. Thus, in combination with computer simulations of cardiac cryo-ablation, our data may be used for predicting the temporal evolution of impedance during ice formation in tissue and might, thus, be used for linking ice-ball or ice-layer dimensions with the actual impedance of a given electrode configuration. To relate size and geometry dependent effects in our analysis, we normalized impedance by its value at body temperature and provided a conversion to conductivity.

5.5. Frequency range

Frequencies used for measuring impedance inside the heart are typically in the order of several kHz to some tens of kHz. For example, a system used in clinical application for electro-anatomical mapping is operated at 8 kHz [32]. A system for assessing catheter wall contact is operated at 25 kHz [33]. Lower frequencies should not be used to avoid interference with intra-cardiac electrograms (band-width up-to 2 kHz) and potential risk of unintended tissue stimulation. Conventional electric impedance tomography is performed at 50 kHz [34]. At frequencies of some 100kHz the quasi-static approximation of volume conduction is no longer applicable, which significantly complicates experimental design and data analysis [35]. Thus, we focused on a central frequency of 20 kHz. Furthermore, we also investigated a lower frequency of 5 kHz and an upper frequency of 80 kHz.

5.6. Limitations of the study

We used standard EP equipment (catheter and cable) for our experiment. The intention was to obtain impedance readings that are comparable to those that might be obtained in a clinical setting. As impedance rises by more than three orders of magnitude when cooling down tissue from body temperature to −50 °C, the parasitic capacitances of the lines mask the tissue properties at very low temperature and high frequency. As a consequence, experimental values are less accurate below −20 °C. This is a limitation, but also an important finding, of our study. As is shown in Appendix C the cable capacitances used for the experiment are representative of those in standard equipment that is used for minimally invasive cardiac electrophysiology.

We applied slow freezing and thawing for reducing temperature gradients inside the tissue. In a clinical environment such slow cooling or thawing rates are unrealistic. Catheters used for routine treatment of atrial fibrillation require 90 s to 5 min for freezing throughout the atrial wall [4,11]. Thus, the ice is growing relatively slowly within an atrial wall of about two millimeters thickness, which seems to be sufficiently slow to achieve ion concentrations near the thermodynamic equilibrium.

For avoiding non-conducting gaps between patches of tissue, physiological saline was added to the probe. As the absolute conductivity of physiological saline solution is significantly above the conductivity of myocardium [22] our results overestimated the contribution of the extracellular space to ohmic conduction. However, our data suggest that the relative temperature dependent increase of conductivity is comparable for the saline solution and tissue. Thus, the bias introduced by adding a saline solution is essentially a relative increase of extracellular conductivity by a constant factor.

6. Conclusion

Progressive freezing of tissue during cryo-ablation is accompanied by a continuously increasing percentage of frozen water content in the aqueous electrolytic intra- and extracellular body liquids. Impedance is a surrogate marker for the frozen water content inside the tissue. We provide data that accurately reflects the temperature dependent increase of impedance in bovine myocardial tissue. It may be a more reliable marker for guiding cryo-ablation therapy than temperature. We also provide data quantifying the effect of progressive freezing on tissue conductivity and surface polarization of electrodes. This data will be useful when performing computer simulations of cyro-ablation in the future.

Funding

This work was funded, in part, by a Connecting AustralianEuropean Science Innovation and Excellent (CAESIE) grant and a Global Connections Fund Bridging Grant from the Academy of Technology and Engineering (ATSE) (Australia). The work was also funded, in part, by the Government of the region Tirol, Austria within a cooperation project entitled: Next Generation CoolLoop.

Ethical approval

In accordance with our institution guidelines samples of bovine myocardium were obtained in frozen condition from a certified animal lab (Tierversuchsanstalt Dr. Gnter Klima, Drre 2, A-6421 Rietz, Austria).

Declaration of Competing Interest

Dr. G. Fischer is a founder and shareholder at AFreeze GmbH. All other authors have no competing interests to declare.

Supplementary material

Supplementary material associated with this article can be found, in the online version, at doi:10.1016/j.medengphy.2019.09.017.

References

[1] Rottner L, Fink T, Kuck KH. Cryoballoon ablation beyond paroxysmal atrial fibrillation. Curr Opin Cardiol 2019;34(1):23–8.
[2] Su W, Orme GJ, Hoyt R, Baker J, Compton S, Fellows C, Harding J, Svinarich JT, Kowalski M, Piedad B, Kenigsberg D, Seger J, Ahmad ZK, Wang P. Retrospective review of arctic front advance cryoballoon ablation: a multicenter examination of second-generation cryoballoon (radicool trial). J Interv Card Electrophysiol 2018;51(3):199–204.
[3] Chun KRJ, Brugada J, Elvan A, Geller L, Busch M, Barrera A, Schilling RJ, Reynolds MR, Hokanson RB, Holbrook R, Brown B, Schluter M, Kuck KH. The impact of cryoballoon versus radiofrequency ablation for paroxysmal atrial fibrillation on healthcare utilization and costs: an economic analysis from the fire and ice trial. J Am Heart Assoc 2017;6(8):e006043.
[4] Stuehlinger M, Hoenig S, Spuller K, Koman C, Stoeger M, Poelzl G, Ulmer H, Pachinger O, Steinwender C. CoolLoop first: a first in man study to test a novel circular cryoablation system in paroxysmal atrial fibrillation. J Atr Fibrillation 2015;8(3):1287.
[5] Zhao X, Chua KJ. Regulating the cryo-freezing region of biological tissue with a controlled thermal device. Med Eng Phys 2014;36(3):325–34.

[6] de Asmundis C, Chierchia GB, La Meir M. Extracardiac ice formation during coolloop cryoablation of atrial fibrillation. Pacing Clin Electrophysiol 2018;41(9):1264–5.
[7] Parikh V, Kowalski M. Comparison of phrenic nerve injury during atrial fibrillation ablation between different modalities, pathophysiology and management. J Atr Fibrillation 2015;8(4):1314.
[8] Kadado AJ, Akar JG, Hummel JP. Luminal esophageal temperature monitoring to reduce esophageal thermal injury during catheter ablation for atrial fibrillation: a review. Trends Cardiovasc Med 2019;29(5):264–71.
[9] Radai MM, Abboud S, Rubinsky B. Evaluation of the impedance technique for cryosurgery in a theoretical model of the head. Cryobiology 1999;38(1):51–9.
[10] Yu TH, Zhou YX, Liu J. Dynamic low-frequency electrical impedance of biological materials subject to freezing and its implementation in cryosurgical monitoring. Int J Thermophys 2003;24(2):513–31.
[11] Avitall B, Kalinski A, Kocheril GS, Lizama KS, Coulombe N, Laske T. Characteristics of ice impedance recorded from a ring electrode placed at the anterior surface of the cryoballoon: novel approach to define ice formation and pulmonary vein isolation. Circ Arrhythm Electrophysiol 2018;11(4):e005949.
[12] Edd JF, Ivorra A, Horowitz L, Rubinsky B. Imaging cryosurgery with EIT: tracking the ice front and post-thaw tissue viability. Physiol Meas 2008;29(8):899–912.
[13] Handler M, Fischer G, Seger M, Kienast R, Nowak CN, Pehboeck D, Hintringer F, Baumgartner C. Computer simulation of cardiac cryoablation: comparison with in vivo data. Med Eng Phys 2013;35(12):1754–61.
[14] Seger M, Fischer G, Handler M, Stoeger M, Nowak CN, Hintringer F, Klima G, Baumgartner C. Achieving elongated lesions employing cardiac cryoablation: a preclinical evaluation study. Cryobiology 2012;65(2):145–50.
[15] Wolf M, Gulich R, Lunkenheimer P, Loidl A. Broadband dielectric spectroscopy on human blood. Biochim Biophys Acta 2011;1810(8):727–40.
[16] Takami M, Misiri J, Lehmann HI, Parker KD, Johnson SB, Sarmiento RI, Packer DL. Spatial and time-course thermodynamics during pulmonary vein isolation using the second-generation cryoballoon in a canine in vivo model. Circ Arrhythm Electrophysiol 2015;8(1):186–92.
[17] Yang F, Tiano J, Mittal S, Turakhia M, Jacobowitz I, Greenberg Y. Towards a mechanistic understanding and treatment of a progressive disease: atrial fibrillation. J Atr Fibrillation 2017;10(3):1627.
[18] Radebaugh R. Heat transfer issues in cryogenic cathers. In: Kakac S, Vasiliev L, Bayazitoglu Y, Yener Y, editors. Microscale heat transfer fundamentals and applications.. Springer, Dordrecht; 2005. p. 445–64.
[19] Prickett RC, Elliott JA, McGann LE. Application of the osmotic virial equation in cryobiology. Cryobiology 2010;60(1):30–42.
[20] Anand G, Lowe A, Al-Jumaily AM. Parametric electrical modelling of human forearm simulation response using multi-frequency electrical bioimpedance. J Biosens Bioelectron 2016;7(2):206.
[21] Grimnes S, Martinsen O. Alpha-dispersion in human tissue. J Phys Conf Ser 2010;224(1):012073.
[22] Johnston BM. Six conductivity values to use in the bidomain model of cardiac tissue. IEEE Trans Biomed Eng 2016;63(7):1525–31.
[23] Sauerheber R, Heinz B. Temperature effects on conductivity of seawater and physiologic saline, mechanism and significance. Chem Sci J 2015;6(4):109.
[24] Skourou C, Hoopes PJ, Paulsen KD. Tissue permittivity: a monitor for progressive tissue fibrosis as observed in bystander tissues following experimental high dose rate irradiation. Cancer Biol Ther 2009;8(23):2223–9.
[25] Yu TH, Liu J, Zhou YX. Using electrical impedance detection to evaluate the viability of biomaterials subject to freezing or thermal injury. Anal Bioanal Chem 2004;378(7):1793–800.
[26] Gage AA, Baust J. Mechanisms of tissue injury in cryosurgery. Cryobiology 1998;37(3):171–86.
[27] Prickett RC, Marquez-Curtis LA, Elliott JA, McGann LE. Effect of supercooling and cell volume on intracellular ice formation. Cryobiology 2015;70(2):156–63.
[28] Gage AA, Baust JM, Baust JG. Experimental cryosurgery investigations in vivo. Cryobiology 2009;59(3):229–43.
[29] Skanes AC, Klein G, Krahn A, Yee R. Cryoablation: potentials and pitfalls. J Cardiovasc Electrophysiol 2004;15(10 Suppl):28–34.
[30] Han B, Bischof JC. Direct cell injury associated with eutectic crystallization during freezing. Cryobiology 2004;48(1):8–21.
[31] Wong T, Markides V, Peters NS, Davies DW. Clinical usefulness of cryomapping for ablation of tachycardias involving perinodal tissue. J Interv Card Electrophysiol 2004;10(2):153–8.
[32] Skala T, Taborsky M. Electromechanical mapping in electrophysiology and beyond. Cor et Vasa 2015;57:e470–81.
[33] Deno DC, Sih HJ, Miller SP, Teplitsky LR, Kuenzi R. Measurement of electrical coupling between cardiac ablation catheters and tissue. IEEE Trans Biomed Eng 2014;61(3):765–74.
[34] Li X, Shin H, Li L, Magat E, Li S, Zhou P. Assessing the immediate impact of botulinum toxin injection on impedance of spastic muscle. Med Eng Phys 2017;43:97–102.
[35] Zhang W, Li D. An instrumental electrode model for solving EIT forward problems. Physiol Meas 2014;35(10):2001–26.
[36] Bodnar RJ. Revised equation and table for determining the freezing point depression of H_2O – NaCl solutions. Geochim Cosmochim Acta 1993;57(3):683–684.